Supporting Information

Tailoring Molecular Orientation to Enhance Photocurrent and Fill Factor in Green-Solvent Processed Organic Solar Cells

Yonglin Cao [a, b], *Khawla Alkhezaim,*[c] *Derya Baran,*[c,d] *Safa shoaee* *[a, b]

a. Heterostructure semiconductor physics, Paul Drude Institute for Solid State Electronics, Hausvogteiplatz 5-7, 10117 Berlin, Germany

b. Institute of Physics and Astronomy, University of Potsdam, Karl-Liebknecht-Str. 24-25, 14476 Potsdam-Golm, Germany

c. Material Science and Engineering Program (MSE), Physical Sciences and Engineering Division, King Abdullah University of Science and Technology (KAUST), Thuwal, 23955-6900, Kingdom of Saudi Arabia

d. Center for Renewable Energy and Storage Technologies (CREST), King Abdullah University of Science and Technology (KAUST), Thuwal, 23955-6900, Saudi Arabia

Email: shoaee@pdi-berlin.de

Experimental Section

Device fabrication

The organic solar cell devices were fabricated with the conventional structure of ITO/PEDOT:PSS /PTB7-Th:BTPV-4F-eC9/PDINN/Ag. The ITO substrates were ultrasonically cleaned using acetone (15 min), Hellmanex (15 min), distill water (20 min) and isopropanol (15 min), and then treated in plasma for 5 min with a power of 200 W. Afterwards, a thin layer of PEDOT:PSS was spin-coated on the cleaned ITO-coated glass substrates with 5000 rpm for 30s. To evaporate the water solvent thoroughly, the PEDOT:PSS thin layers were annealed at 150 °C for 20 min. Then, the ITO substrates were transferred to a glovebox. A blend of PTB7-Th and BTPV-4F-eC9 with a weight ratio of 1:1.5 were dissolved in chloroform, toluene and o-xylene solvents, respectively. The weight ratio of PAT to acceptor was 10% and 20%. Then the solutions were prepared inside a nitrogen-filled glovebox and stirred for 3 hours at corresponding temperature with a total concentration of 16 mg/ml in chloroform (40 °C), 16 mg/ml in toluene (40 °C) and 20 mg/ml in o-xylene solvents (60 °C). The active layer was spin-coated from the blend solution at room temperature at corresponding rpm for 40s to form a corresponding thickness active layer (the details are shown in Table S1). Afterwards, the active layer was thermal annealed at corresponding temperature for 10 min (110 °C for chloroform, 150 °C for toluene and 150 °C for o-xylene). Then, a thin layer of PDINN in methanol solution at 1 mg/ml was spin-coated at 2000 rpm for 40s and the 100nm Ag was deposited as the electrode by thermal evaporation to complete the device with an active area of 0.06 cm^2 (0.01 cm^2 for small pixel devices), which is defined by the metal shadow mask and the patterned ITO.

Table S1. The spin coating rate for active layer

Solvent	chloroform				toluene				o-xylene			
Thickness (nm)	80	95	110	125	80	95	110	125	80	95	110	125

Spin coating rate (rpm)	3750	3125	2575	2000	3250	2500	1750	1000	3750	2825	1900	1250

Current density-voltage characteristics (J-V)

The J-V characteristics were measured by using a Keithley 2400 system with a filtered Oriel Sol2A Class AA Xenon lamp, which is simulated AM1.5G irradiation at 100 mWcm-2. The temperature of the measured devices was controlled at 25 °C.

External quantum efficiency (EQE_{pv})

The EQE_{pv} was measured with a 300 W Philips halogen lamp and the light was chopped by 80 Hz with a chopper and gets monochromated with an Oriel 260 Monochromator. The EQE_{PV} spectrum was calibrated with a silicon diode (Newport UV 818) for below 1100nm wavelength and with an InGaAs diode (Newport IR 918) for above 1100nm wavelength. An SR 830 Lock-In Amplifier measures the response of the solar cell under different bias voltages applied by a Keithley 2400.

UV-vis absorption measurements

Firstly, the samples were encapsulated with a thin transparent glass. Then using Cary 5000 with an integrating sphere, the encapsulated film was placed at the transmittance port for transmittance (T%) measurement and then at the reflectance port for reflectance (R%). Optical density is calculated via

OD = lg((100-R%)/T%), where, OD is the optical density.

Photoluminescence (PL) and Photoluminescence quantum yield (PLQY)

For the PL measurements, the samples were encapsulated by thin transparent films along the edges. An Andor Solis 803 System composed of mirrors and filters was used. A silicon detector with an 800 nm center wavelength (CWL) grid and an InGaAs detector with 1100 and 1400 nm CWL grids were equipped to detect the PL intensity. An excitation wavelength of 520 nm laser was used and the light was adjusted to a certain intensity, which was kept the same for all the samples. PL spectra were recorded with different gratings with CWL of 800, 1100, and 1400 nm and merged afterwards.

For the PLQY measurements, the samples were covered with a plastic mask to avoid the waveguiding effect. The measurements were performed inside an integrating sphere (Hamamatsu Photonics K.K. A10094) under the illumination of a 520 nm continuous laser (InsaneWare). The intensity of the laser was adjusted to 1 sun condition using a Si photodiode. PLQY can be calculated as the ratio of the number of photons emitted (Nemi) to the number of photons absorbed (Nabs) by the samples. The emitted and absorbed photons can be determined by performing different measurements.

1. Without sample in the integrating sphere, with laser filter for remaining laser correction.
2. With sample in the integrating sphere, without laser filter for absorption.
3. Without sample in the integrating sphere, without laser filter for absorption correction.
4. With sample in the integrating sphere, with laser filter for emission.

An additional dark measurement with the laser shutter closed is performed for background correction for all measured spectra.

Bias-assisted charge extraction (BACE)

An excitation wavelength of 520 nm laser was used for illumination. During illumination, the small-pixel-area (0.01 cm2) device was kept at the equivalent V_{OC} using an Agilent 81150A pulse generator.

Right after switching off the laser, a reverse bias was applied to the device by the same pulse generator (Agilent 81150A), allowing a fast charge extraction time of 10-20 ns. The transient current was measured via a 50 Ω resistor in series with the device and recorded by an oscilloscope (Agilent DSO9104H).

Time-delayed collection field (TDCF)

The small-pixel-area (0.01 cm2) device was excited with a laser pulse at 532nm from a diode pumped, Q-switched Nd:YAG laser (NT242, EKSPLA) with a ~6 ns pulse duration at a typical repetition rate of 500 Hz. The laser pulse was delayed and homogeneously scattered in an 85 m long silica fiber (LEONI) to compensate for the internal latency of the pulse generator. Charges were generated while the device was held at different pre-bias (V_{pre}). After a delay time, a high reverse collection bias (V_{coll}), was applied to extract the charges in the device. V_{pre} and V_{coll} were set by an Agilent 81150A pulse generator through a home-built amplifier, which was triggered by a fast photodiode (EOT, ET-2030TTL). The current from the device was measured via a 50 Ω resistor in series with the sample and recorded with an oscilloscope (Agilent DSO9104H). To ensure that non-geminate recombination losses are insignificant during the measurement, a sufficiently large V_{coll} of -2.5 V was applied and a low laser intensity was kept ensuring that the extracted charge is proportional to the laser fluence.

Electroluminescence (EL) and electroluminescence quantum yield (ELQY)

For EL measurements, a constant voltage was applied to the device using a Keithley 2400 to reach the same current density as the short-circuit current density under AM 1.5G, 100 mW cm-2. Emission spectra were recorder by an Andor Solis 803 System with a silicon and InGaAs detector. EL spectra were recorded with different gratings with CWL of 800, 1100 and 1400 nm and merged afterwards.

For ELQY measurements, a Hamamatsu silicon photodiode 1010B was placed in front of the measured pixel with a distance smaller than 0.5 cm. A Keithley 485 Picoammeter was connected to the detector and used to measure the emitted light intensity. A Keithley 2400 SourceMeter was used to apply the voltage and record the injected current. ELQY can be calculated via

$$ELQY = \frac{J_{detector}}{J_{injection}} \times C$$

Where $J_{detector}$ is the photocurrent of the detector, $J_{injection}$ is the injected current of the device, C is the conversion factor, considering the emission spectrum of the device and the external quantum efficiency of the detector.

Resistance dependent photovoltage (RPV)

The laser pulse comes from a diode pumped, Q-switched Nd:YAG laser (NT242, EKSPLA) with a ~5ns pulse duration at a frequency of 500 Hz. Low laser pulse fluences were used to avoid screening of the internal field by photogenerated charge carriers, and build-up of charges inside the device. The change in electrostatic potential across the device due to transport of charges was amplified by a Femto HVA amplifier (model HVA-200M-40-F), and the photovoltage transients were recorded by an oscilloscope (Agilent DSO9104H) with a load resistance of 1M ohm.

Grazing Incidence Wide-Angle X-ray Scattering (GIWAXS)

GIWAXS measurements were performed using Xenocs Xeuss 3.0 equipped with a Genix 3D Cu source with focused collimation, λ = 1.54 Å and an EIGER2 R 4M detector. The sample-to-detector-distance was set to 130 mm. The incidence angle of the X-ray beam with respect to the sample plane was 0.12°. Collection was carried out in a vacuum. All GIWAXS data processing was performed using a custom

Python batch script, initially developed by Zapata-Arteaga, O., et al.[1] and integration was implemented using PyFAI modules.[2] The peak analysis was handled through a custom batch processing fitting script, utilizing the irsqr method for baseline corrections from the Pybaselines module.[3] All baseline parameters, such as lambda and quantiles, were kept identical across all datasets to ensure consistency. Peak locations were detected using the "SciPy.signal" function, and the fitting was carried out via least-squares routine using the LMFIT module. [4]

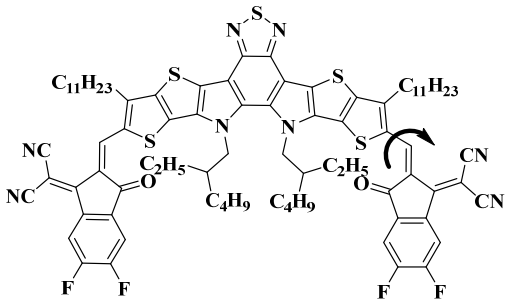

Figure S1. Chemical structures of the NFA small molecule, Y6.

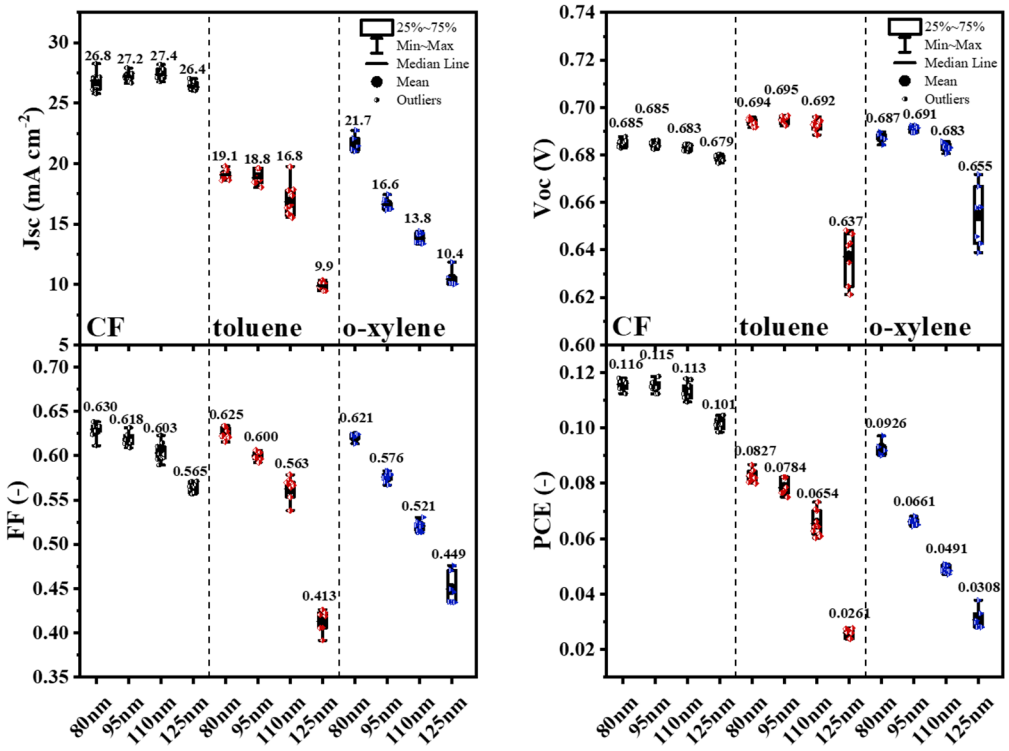

Figure S2. The box diagram of photovoltaic parameters obtained from current-voltage measurements under simulated AM 1.5G, 100 mW cm-2 illumination of OSCs based on PTB7-Th:BTPV-4F-eC9 thickness-dependent system processed in three kinds of solvents.

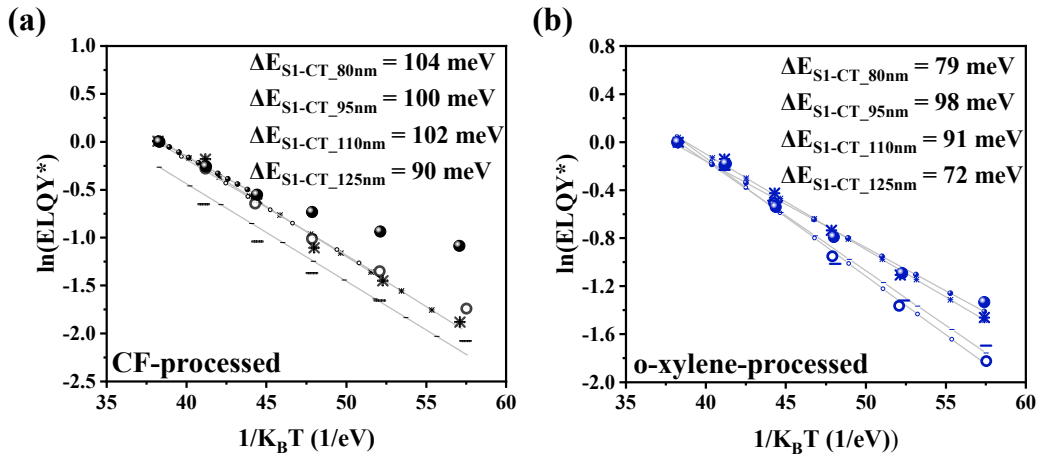

Figure S3. Temperature-dependent ELQY values of (a) the CF-processed thickness-dependent system and (b) the o-xylene-processed thickness-dependent system.

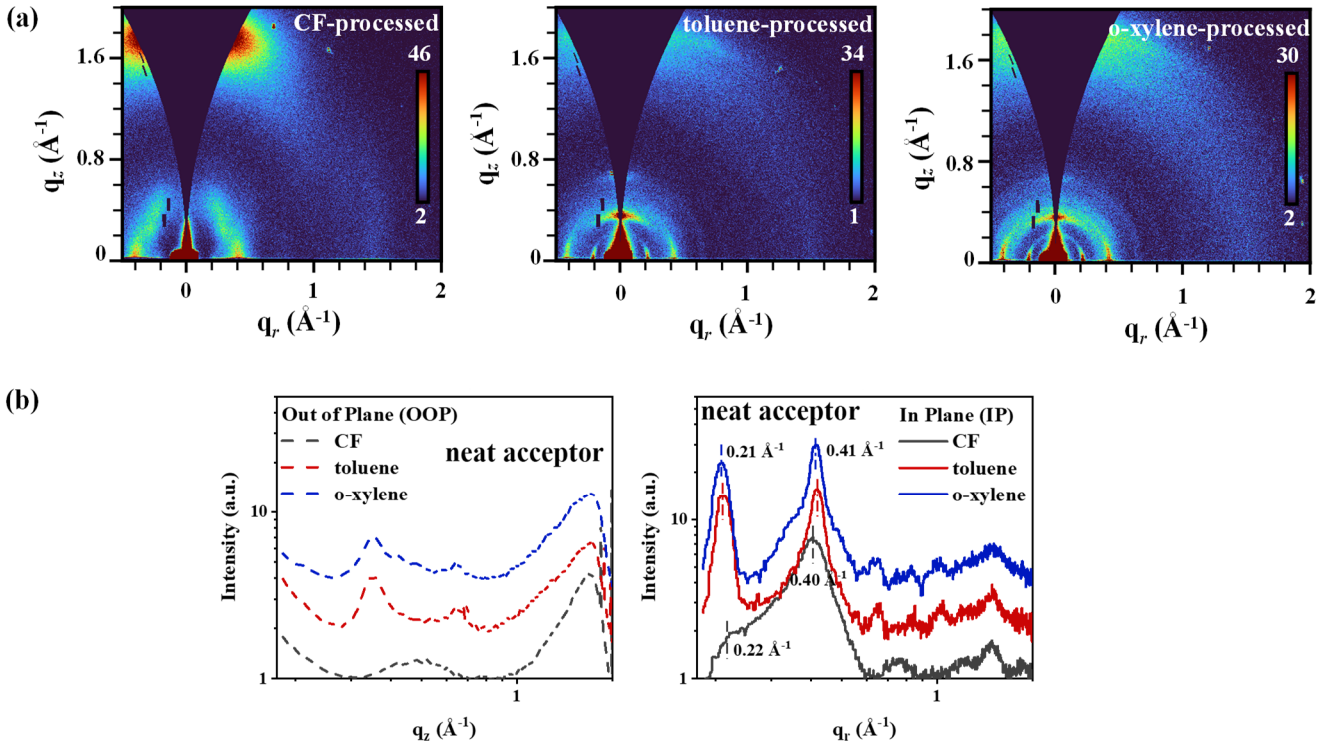

Figure S4. (a) 2D-GIWAXS pattern and (b) corresponding line-cut profiles along the out of plane (OOP) and in plane (IP) directions of the neat acceptor film processed with CF, toluene and o-xylene solvents.

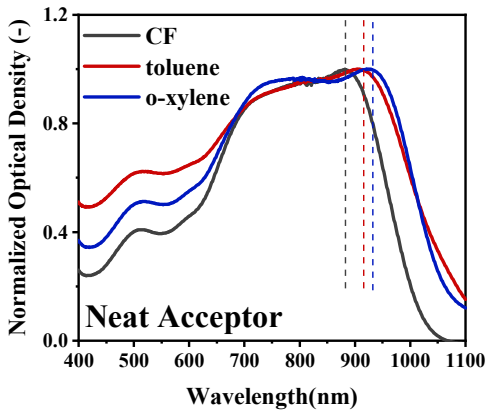

Figure S5. normalized optical density spectra of the neat acceptor film processed with CF, toluene and o-xylene solvents. The dashed line in the figure marks the position of the peak 1.

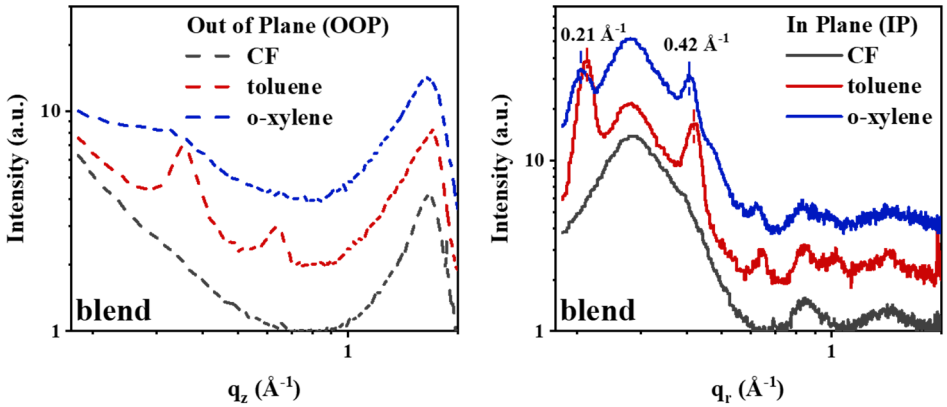

Figure S6. Corresponding line-cut profiles along the out of plane (OOP) and in plane (IP) directions of the blend film processed with CF, toluene and o-xylene solvents at an active layer thickness of 80 nm.

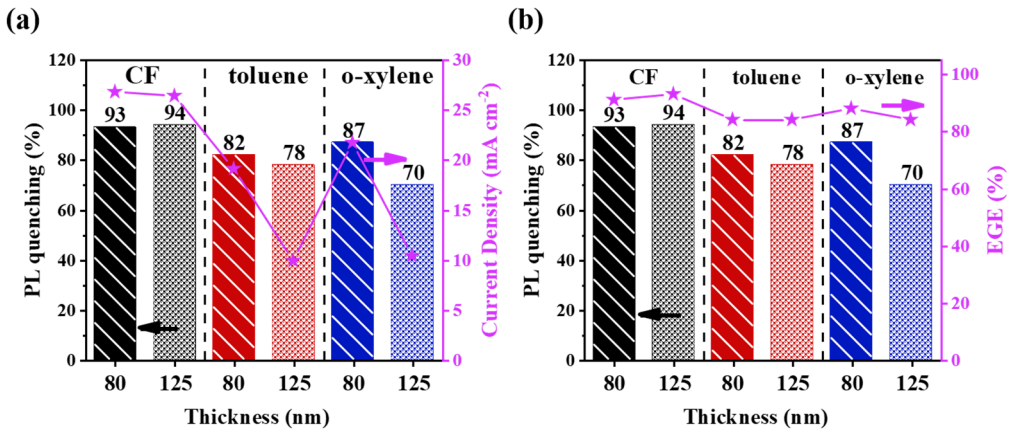

Figure S7. PL quenching of the acceptor in blend films of varying thicknesses fabricated using different solvents, shown alongside (a) current density from the J–V characteristics of the devices and (b) external generation efficiency (EGE) from TDCF measurements.

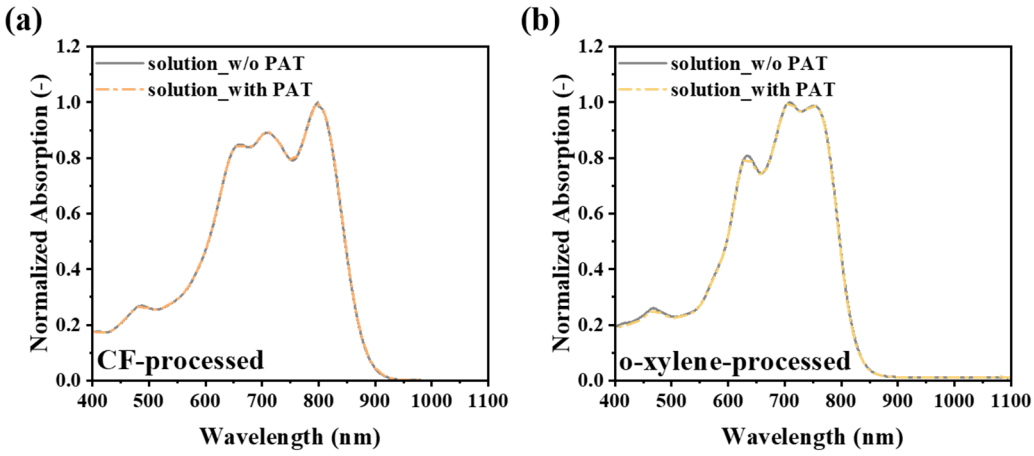

Figure S8. Effects of PAT treatment on normalized solution absorption spectra for (c) the CF-processed system and (b) the o-xylene-processed system.

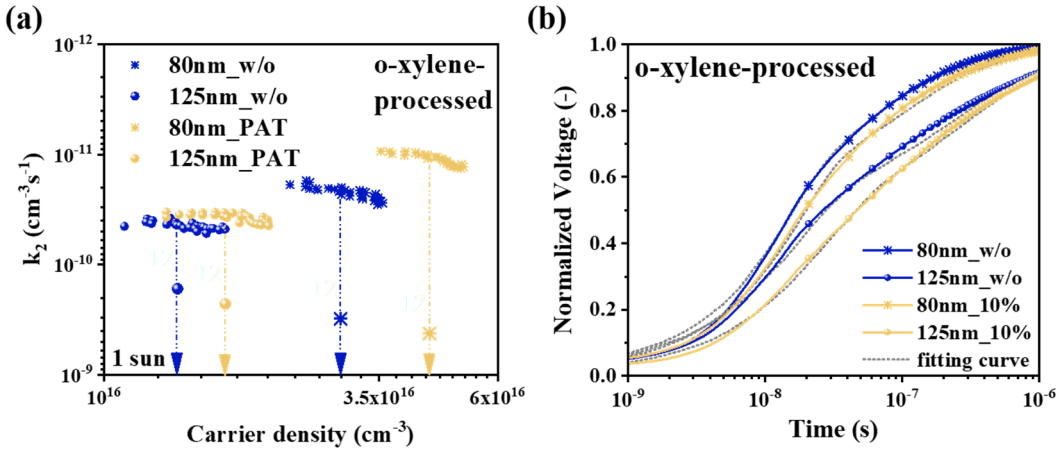

Figure S9. (a) Bimolecular recombination coefficient versus charge carrier density, (b) resistance-dependent photovoltage results, determined using a python fitting code to the photovoltage rise, for o-xylene-processed thickness-dependent with and without PAT system.

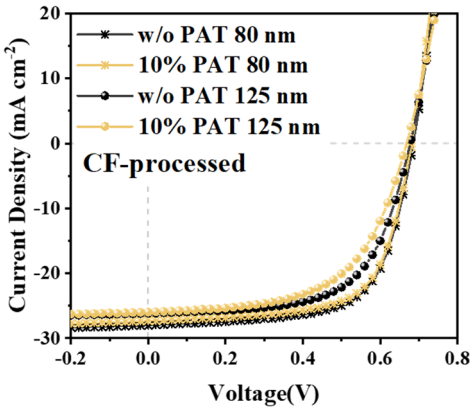

Figure S10. The current-voltage (JV) characteristics of the CF-processed system using PAT as additive under AM 1.5 G illumination at 100 mW cm^{-2}.

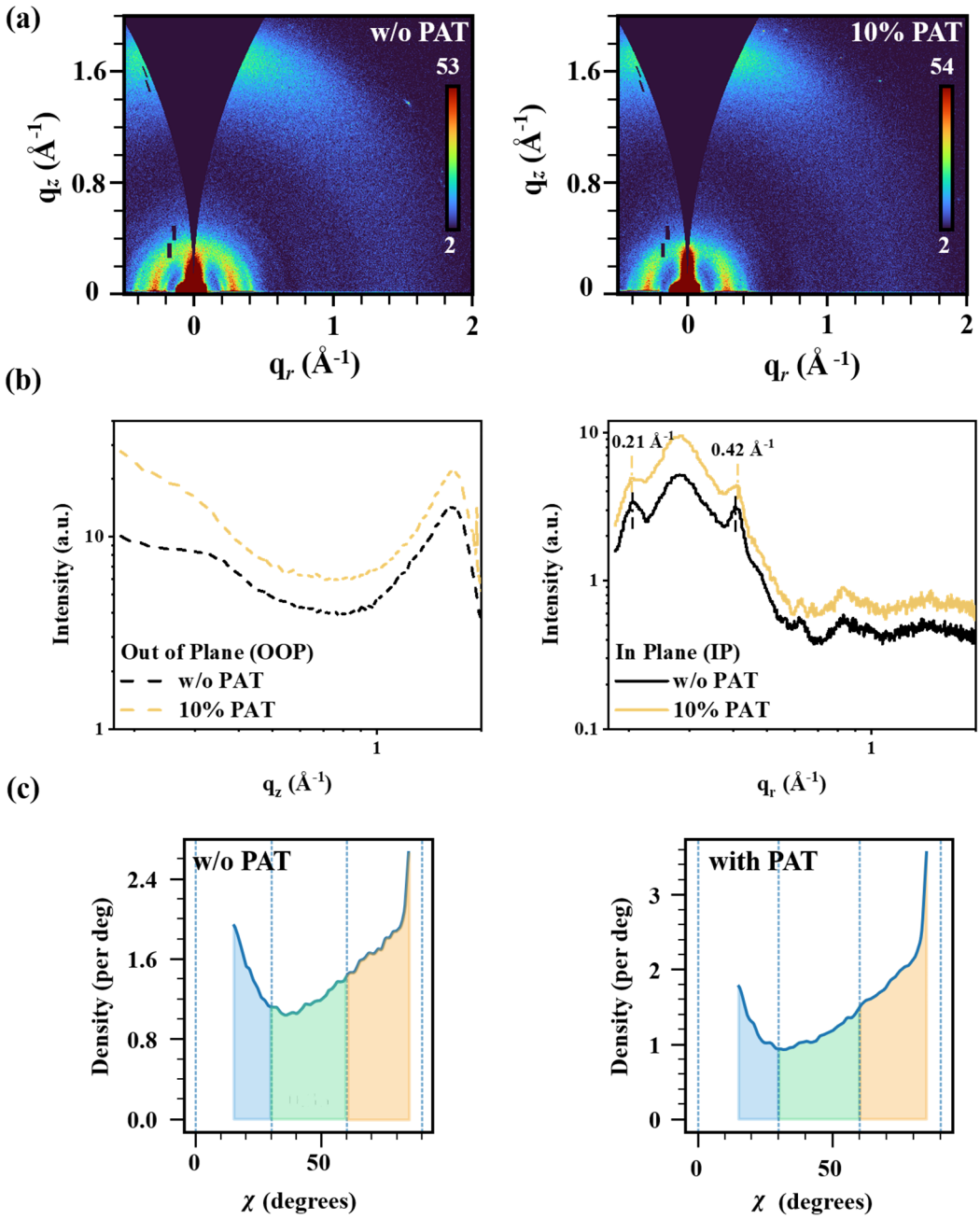

Figure S11. (a) 2D-GIWAXS pattern, (b) corresponding line-cut profiles along the out of plane (OOP) and in plane (IP) directions and (c) chi-profiles in the lamellar region at q = 2.5 nm^{-1} (χ = 0°, out of plane; χ = 90°, in plane) of the blend film processed with o-xylene solvents, with and without additive.

Table S2. Crystalline parameters of neat acceptor films calculated from GIWAXS.

Neat	π-π Stacking			
Acceptor	q (Å^{-1})	d (Å)	L (Å)	q (Å^{-1})
CF	1.67	3.76	20.2	0.22
				0.40
toluene	1.61	3.91	23.4	0.21
				0.41
o-xylene	1.68	3.96	19.5	0.21
				0.41

Table S3. Crystalline parameters of blend films calculated from GIWAXS.

blend	π-π Stacking			q (Å^{-1})	I_{IP}/I_{OOP}
	q (Å^{-1})	d (Å)	L (Å)		
CF	1.67	3.77	17.6	-	-
				-	-
toluene	1.68	3.74	26.6	0.21	6.5
				0.42	5.2
o-xylene	1.68	3.75	16.8	0.21	3.7
				0.42	4.9
o-xylene with additive	1.69	3.73	17.4	0.21	2.1
				0.42	4.8

Table S4. The carrier density (n_{cs}) under 1 sun condition from BACE measurement are tabulated, along with the carrier density ratio change(1-n_{cs}_125nm/n_{cs}_80nm) comparing devices with active layer thicknesses of 80 nm and 125 nm.

	$n_{cs}[cm^{-3}]$		*Change [%]*
Thickness [nm]	80	125	
CF	2.1×10^{16}	1.8×10^{16}	14%
toluene	1.7×10^{16}	1.0×10^{16}	41%
o-xylene	1.7×10^{16}	8.9×10^{15}	48%

Table S5. The faster and slower carrier mobility values (μ_f and μ_s) for varying thicknesses devices are calculated from RPV measurements.

	μ_s [$cm^2\ V^{-1}\ s^{-1}$]				μ_f [$cm^2\ V^{-1}\ s^{-1}$]			
Thickness [nm]	80	95	110	125	80	95	110	125
CF	9×10^{-4}	4×10^{-4}	4×10^{-4}	5×10^{-4}	7×10^{-3}	2×10^{-3}	3×10^{-3}	3×10^{-3}
toluene	8×10^{-4}	8×10^{-4}	6×10^{-4}	4×10^{-4}	6×10^{-3}	1×10^{-2}	9×10^{-3}	6×10^{-3}
o-xylene	1×10^{-4}	1×10^{-4}	1×10^{-4}	3×10^{-4}	2×10^{-3}	3×10^{-3}	3×10^{-3}	4×10^{-3}

Table S6. Bimolecular recombination coefficient of o-xylene-processed thickness-dependent with and without PAT system, measured with bias-assisted charge extraction, and the faster and slower carrier mobility values (μ_f, μ_s) are calculated from RPV measurement, are tabulated together with the Langevin reduction factor according to the equation $\gamma=k_2/k_L$.

Thickness [nm]	Additive	k_2 [$cm^3\ s^{-1}$]	μ_s [$cm^2\ V^{-1}\ s^{-1}$]	μ_f [$cm^2\ V^{-1}\ s^{-1}$]	γ
80	w/o	2×10^{-11}	2×10^{-4}	3×10^{-3}	0.012
125	w/o	4×10^{-11}	1×10^{-4}	7×10^{-3}	0.011
80	10%	1×10^{-11}	1×10^{-4}	3×10^{-3}	0.006
125	10%	4×10^{-11}	1×10^{-4}	3×10^{-3}	0.025

Table S7. Voltage Loss Analysis

	$E_{gap,A}/q$ (V)	ΔVoc^{rad} (V)	Voc^{SQ} (V)	$\Delta Voc^{rad,\ bg}$ (V)	Voc^{rad} (V)	$\Delta Voc^{non\text{-}rad}$ (V)	Voc (V)	ΔVoc^{total} (V)
CF_80nm	1.28	0.26	1.02	0.06	0.96	0.27	0.69	0.59
CF_125nm	1.27	0.26	1.01	0.04	0.97	0.29	0.68	0.59
toluene_80nm	1.27	0.26	1.01	0.05	0.96	0.27	0.69	0.58
toluene_125nm	1.26	0.26	1.00	0.05	0.95	0.31	0.64	0.62
o-xylene_80nm	1.27	0.26	1.01	0.05	0.96	0.27	0.69	0.58
o-xylene_125nm	1.26	0.26	1.00	0.04	0.96	0.30	0.66	0.60

Voltage Losses Analysis

To assess the voltage loss in the thickness-dependent solvent-processed systems, we measured the electroluminescence quantum yield (ELQY) as a function of the injected current, as shown in Supporting Information. The total voltage loss analysis is tabulated in Table S2 and the details of calculation are shown in Supporting Information. We found that as the film thickness increase from 80nm to 125nm, a total voltage loss (ΔVoc^{total}) of CF-processed system increases from 46% to 47%, with an increase from 46% to 49% loss in toluene-processed system and from 46% to 48% in o-xylene-processed system. In solvent-processed system, we obtain the same radiative loss of 0.26 eV and the similar radiative recombination below the gap $\Delta Voc^{rad, bg}$ as a function of thickness. Non-radiative Voc losses ($\Delta Voc^{non\text{-}rad}$) can be calculated with $q\Delta Voc^{non\text{-}rad} = -k_B T ln(ELQY)$, where q is the elementary charge, k_B is the Boltzmann constant and T is the kelvin temperature. The largest $\Delta Voc^{non\text{-}rad}$ is calculated for toluene-processed system in thicker film (0.31eV), followed by o-xylene-processed system (0.30 eV) and the lowest value of 0.29 eV is estimated for CF-processed system.

The estimated Voc in the radiative limit (Voc^{SQ}), assuming an ideal step-like EQEpv, which is 1 above and 0 below the bandgap of the system, can be calculated as

$$Voc^{SQ} = \frac{K_B T}{q} ln \frac{Jsc^{SQ}}{J_{0,rad}^{SQ}} \qquad \text{Equation S1}$$

Where K_B is the Bolzmann constant, T is the temperature, Jsc^{SQ} is the short-circuit current density integrated from the product of the ideal EQEpv spectrum and the solar AM 1.5G, 100 mW cm^{-2} spectrum, $J_{0,rad}^{SQ}$ is the radiative limit of the dark current integrated from the product of the ideal EQEpv spectrum and black body emission spectrum at room temperature.

If only radiative recombination would occur in the device, V_{OC} would reach the upper limit (Voc^{rad}), which can be calculated as

$$Voc^{rad} = \frac{K_B T}{q} ln \frac{Jsc}{J_{0,rad}}$$ Equation S2

where, *Jsc* is the short-circuit current density under illumination (AM 1.5G, 100 mW cm^{-2}), $J_{0,\,rad}$ is the radiative limit of the dark current integrated from the product of the device EQE_{PV} spectrum and black body emission spectrum at room temperature.

Radiative voltage losses (ΔVoc^{rad}) can be calculated as

$$\Delta Voc^{rad} = \frac{E_{gap,A}}{q} - Voc^{SQ}$$ Equation S3

The radiative loss below bandgap ($\Delta V_{OC}^{rad,\,bg}$) can be calculated as the difference between Voc^{SQ} and Voc^{rad},

$$\Delta Voc^{rad,bg} = Voc^{SQ} - Voc^{rad}$$ Equation S4

Non-radiative voltage losses ($\Delta Voc^{non\text{-}rad}$) can be calculated as

$$\Delta Voc^{non-rad} = -\frac{K_B T}{q} lnELQY$$ Equation S5

The total voltage losses can be calculated as the sum of all voltage losses via

$$\Delta Voc^{total} = \Delta Voc^{rad} + \Delta Voc^{rad,bg} + \Delta Voc^{non-rad}$$ Equation S6

RPV Data Simulation

Assuming that each charge carrier contributes independently to the overall photovoltage, it becomes feasible to fit their respective influences separately and subsequently sum their contributions to reconstruct the full RPV curve. This is only possible if the curves show a separation of the first regime, the one where both carriers contribute to the voltage and the second regime where one assumes only a contribution of the slower carriers.

1. Time correction

RPV-curves rely on a logarithmic scaling of the time axis, making the accurate determination of the curve's starting point essential for the early curve shape. Theoretical studies have shown that the initial rise in voltage is approximately linear with time. However, this rise is often preceded by a slower increase, primarily attributed to experimental artifacts such as the shape of the laser pulse. To correct for this, the linear portion of the early-time voltage rise can be extrapolated backward to determine the theoretical onset of the experiment. This extrapolated intercept then serves as a corrected time zero.

2. Second Regime fit

In the second regime, only the slower carriers contribute to the voltage increase therefore making it easier to identify disorder and mobility. The simulation curves need to be shifted to matches the experimental curve. Disorder and mobility can then be read and calculated. Often it is not clear which curve is the best choice especially when oscillation and other experimental artifacts are present. In order to automate this process, it is necessary to define a quantity for the similarity between two curves. We use the mean squared error (MSE) as the quantity. This change was necessary because extensive testing revealed issues with the previous metric. To use the MSE effectively, a time correction factor must first be determined so that the curves align properly before calculating the MSE.

3. First Regime fit

After finding a matching curve one can interpolate the simulation and experimental curve to isolate only the fast carrier, by subtracting both curves. This time the simulation curve needs to be normalized to 0.5 to account only for one type of carrier. After the transformation the fitting of the first regime is the same as for the second one.

4. Reconstruction

After obtaining all parameters from the first and second regime fits, the experimental RPV curve can be reconstructed using only simulation data. First, the time axis is corrected, then the curves are normalized to 0.5, interpolated to ensure matching time points and finally added together. When plotted alongside the experimental data, one can visually assess whether the simulated and experimental curves align.

References

1 O. Zapata-Arteaga,A. Perevedentsev,M. Prete,S. Busato,P. S. Floris,J. Asatryan,R. Rurali,J. Martín,M. Campoy-Quiles. *ACS Energy Lett.* 2024, **9**, 3567-3577.

2 J. Kieffer,D. Karkoulis. *Journal of Physics: Conference Series* 2013, **425**, 202012.

3 D. Erb, **2025**, DOI 10.5281/ZENODO.5608581.

4 M. Newville, T. Stensitzki, D. B. Allen, A. Ingargiola, **2014**, DOI 10.5281/ZENOD- O.11813